Mon. Not. R. Astron. Soc. **331,** 98–110 (2002)

The universal mass accretion history of cold dark matter haloes

Frank C. van den Bosch★

Max-Planck-Institut für Astrophysik, Karl Schwarzschild Str. 1, Postfach 1317, 85741 Garching, Germany

Accepted 2001 November 13. Received 2001 November 2; in original form 2001 May 15

ABSTRACT

We use the extended Press–Schechter formalism to investigate the rate at which cold dark matter haloes accrete mass. We discuss the shortcomings of previous methods that have been used to compute the mass accretion histories of dark matter haloes, and present an improved method based on the *N*-branch merger tree algorithm of Somerville & Kolatt. We show that this method no longer suffers from inconsistencies in halo formation times, and compare its predictions with high-resolution *N*-body simulations. Although the overall agreement is reasonable, there are slight inconsistencies which are most easily interpreted as a reflection of ellipsoidal collapse (as opposed to spherical collapse assumed in the Press–Schechter formalism). We show that the average mass accretion histories follow a simple, universal profile, and we present a simple recipe for computing the two scale-parameters which is applicable to a wide range of halo masses and cosmologies. Together with the universal profiles for the density and angular momentum distributions of cold dark matter haloes, these universal mass accretion histories provide a simple but accurate framework for modelling the structure and formation of dark matter haloes. In particular, they can be used as a backbone for modelling various aspects of galaxy formation where one is not interested in the detailed effects of merging. As an example we use the universal mass accretion history to compute the rate at which dark matter haloes accrete mass, which we compare with the cosmic star formation history of the Universe.

Key words: stars: formation – galaxies: formation – galaxies: haloes – cosmology: theory – dark matter.

1 INTRODUCTION

In the standard cold dark matter (CDM) family of cosmological models, dark matter haloes form hierarchically through the accretion and merging of smaller structures that condense out of a Gaussian initial density field. The rate at which these dark matter haloes grow in mass sets, amongst others, the rate at which baryons can cool to form luminous objects. Therefore, knowledge of the mass accretion rate of dark matter haloes is an essential ingredient in our cosmological framework of structure formation.

Since the collapse and virialization of dark matter haloes is a non-linear process, one generally resorts to numerical *N*-body simulations to study the formation and evolution of structures in a CDM universe. However, this method has a number of important drawbacks. First of all, numerical simulations are computationally expensive, making it unfeasible to explore a wide range of cosmological models. Secondly, computational limitations only allow simulations of small volumes and/or a small dynamical mass range. This makes it virtually impossible to follow simultaneously the formation and evolution of objects from sub-galactic scales up to the scale of (super)clusters.

An important alternative is provided by the Press–Schechter (PS) formalism (Press & Schechter 1974) which allows a much faster exploration of halo mass accretion histories for a wide range of cosmologies and masses. In addition, the PS formalism provides a framework that allows us to gain insights into the physical processes involved. The main ansatz of the PS formalism is to consider the initial density field extrapolated *linearly* to redshift z and smoothed on some typical mass scale M. Regions above a certain threshold value are then associated with collapsed objects of mass M at redshift z. Motivated by Birkhoff's theorem, it is therefore assumed that the non-linear evolution of density perturbations, described by means of a spherical 'top hat' model (Gunn & Gott 1972), does not influence the remainder of the universe. Press & Schechter (1974) used this formalism to compute the mass function of dark matter haloes as function of redshift, which has been found to be in remarkably good agreement with results from *N*-body simulations (e.g. Efstathiou et al. 1988; Carlberg & Couchman 1989; Lacey & Cole 1994; Gelb & Bertschinger 1994; Ma 1996).

The PS theory has been extended to give the *conditional*

★E-mail: vdbosch@mpa-garching.mpg.de

probabilities $P(M_2, z_2|M_1, z_1)$ that a given particle at redshift z_1 inside a halo of mass M_1 at an earlier time z_2 was embedded in a halo of mass M_2 (Bond et al. 1991; Bower 1991; Lacey & Cole 1993, hereafter LC93). This extended Press–Schechter (hereafter EPS) formalism is easily manipulated to yield merger rates, halo formation/survival times and various other statistics (LC93). Of particular importance has been the construction of halo merger trees (e.g. Cole & Kaiser 1988; Kauffmann & White 1993; Somerville & Kolatt 1999; Sheth & Lemson 1999), which are widely used in semi-analytical models for the formation of galaxies (e.g. Kauffmann, White & Guiderdoni 1993; Somerville & Primack 1999; Cole et al. 1994, 2000).

In some cases, however, one is not interested in knowing the detailed distribution of halo progenitor masses, but merely wants to know the rate at which the halo mass increases with time. For instance, in the disc galaxy formation models of Firmani & Avila-Reese (2000) and van den Bosch (2001, 2002), the assumption is explicitly made that haloes accrete their mass smoothly: i.e. one ignores the fact that mass accretion involves the merging of progenitor haloes. In the case of disc galaxies this simplification is permitted, since the fragility of discs suggests that mergers have not played an important role. In this paper we therefore use the EPS formalism to construct average mass accretion histories of dark matter haloes, which we define as the ensemble average $\langle M(z)/M_0\rangle$. Here $M(z)$ is the halo mass as function of redshift and M_0 is the present-day mass of the halo. The main motivation for this study is to investigate whether a simple, universal form exists for $\langle M(z)/M_0\rangle$. Together with the universal profiles for the density distribution (Navarro, Frenk & White 1997) and angular momentum (Bullock et al. 2001) of CDM haloes, such a universal mass accretion history provides a complete description of the structure and evolution of dark matter haloes, which can be used as a framework for detailed modelling of the formation of galaxies. In addition, it is to be expected that the accretion history of dark matter haloes is directly linked to the cosmic star formation history. A universal mass accretion history might therefore prove useful in trying to understand the rapidly improving observations of the star formation rates as function of redshift.

This paper is organized as follows. In Section 2 we start with a brief description of the PS formalism and its extension based on the excursion set formalism. Next, in Section 3 we describe an improved method for computing mass accretion histories, which we test against high-resolution N-body simulations in Section 4. In Section 5 we derive a simple, universal fitting formula for the average mass accretion histories of dark matter haloes, which is applicable to a wide range of halo masses and cosmologies. In Section 6 we discuss a comparison of star formation and halo mass accretion rates, and we conclude in Section 7. A step-by-step recipe for computing the average mass accretion history for a dark matter halo of given mass and in a given cosmology is presented in Appendix A. Finally, in Appendix B we compare our results with those of Wechsler et al. (2001).

2 THEORETICAL BACKGROUND

In the standard model for structure formation, the density field $\delta(\boldsymbol{x}) = \rho(\boldsymbol{x})/\bar{\rho} - 1$ is considered to be a Gaussian random field, which is therefore completely specified by the power spectrum $P(k)$. As long as $\delta \ll 1$ the growth of the perturbations is linear and $\delta(\boldsymbol{x}, t_2) = \delta(\boldsymbol{x}, t_1)D(t_2)/D(t_1)$, where $D(t)$ is the linear growth factor. Once $\delta(\boldsymbol{x})$ exceeds a critical threshold $\delta^0_{\rm crit}$, non-linear effects become important and the perturbation will start to collapse to form a virialized object (halo). In what follows we define δ_0 as the initial density field linearly extrapolated to the present time. In terms of δ_0, regions that have collapsed to form virialized objects at redshift z are then associated with those regions for which $\delta_0 > \delta_{\rm c}(z) \equiv \delta^0_{\rm crit}/D(z)$.[1]

In order to assign masses to these collapsed regions, the PS formalism considers the density field δ_0 smoothed with a spatial window function (filter) $W(r;R_{\rm f})$, where $R_{\rm f}$ is a characteristic size of the filter. There is a considerable amount of freedom in choosing a window function, and here we adopt the often used spatial top-hat filter

$$W(r;R_{\rm f}) = \begin{cases} 3/(4\pi R_{\rm f}^3) & (r \le R_{\rm f}), \\ 0 & (r > R_{\rm f}) \end{cases} \tag{1}$$

The main advantage of this filter over, for example, a Gaussian filter or a k-space top-hat filter is that it is straightforward to compute the mass contained within the window function: $M = 4\pi\bar{\rho}R_{\rm f}^3/3$, with $\bar{\rho}$ the mean mass density of the universe. The ansatz of the PS formalism is that the probability that the density field smoothed with $W(r;\,R_{\rm f})$ exceeds $\delta_{\rm c}(z)$ is the same as the fraction of mass that at redshift z is contained in haloes with masses greater than M. This results in the well-known unconstrained PS mass function for the comoving mass density of haloes:

$$\frac{{\rm d}n}{{\rm d}\ln M}(M,z)\,{\rm d}M = \sqrt{\frac{2}{\pi}}\bar{\rho}\frac{\delta_{\rm c}(z)}{\sigma^2(M)}\left|\frac{{\rm d}\sigma}{{\rm d}M}\right|\exp\left[-\frac{\delta_{\rm c}^2(z)}{2\sigma^2(M)}\right]{\rm d}M \tag{2}$$

(Press & Schechter 1974). Here $\sigma^2(M)$ is the mass variance of the smoothed density field given by

$$\sigma^2(M) = \frac{1}{2\pi^2}\int_0^\infty P(k)\hat{W}^2(k;R_{\rm f})k^2\,{\rm d}k, \tag{3}$$

with $\hat{W}(k;\,R_{\rm f})$ the Fourier transform of $W(r;\,R_{\rm f})$, which for the spatial top-hat filter used here is given by

$$\hat{W}(k;R_{\rm f}) = \frac{3}{(kR_{\rm f})^3}[\sin(kR_{\rm f}) - kR_{\rm f}\cos(kR_{\rm f})]. \tag{4}$$

The EPS model developed by Bond et al. (1991) is based on the excursion set formalism. For each point one constructs 'trajectories' $\delta(M)$ of the linear density field at that position as function of the smoothing mass M. In what follows we adopt the notation of LC93 and use the variables $S = \sigma^2(M)$ and $\omega = \delta_{\rm c}(z)$ to label mass and redshift, respectively. In the limit $R_{\rm f} \to \infty$ one has that $(S, \omega) = (0, 0)$, which can be considered the starting point of the trajectories. Increasing S corresponds to decreasing the filter mass M, and $\delta(S)$ starts to wander away from zero, executing a random walk. The fraction of matter in collapsed objects in the mass interval M, $M + {\rm d}M$ at redshift z is now associated with the fraction of trajectories that have their *first upcrossing* through the barrier $\omega = \delta_{\rm c}(z)$ in the interval S, $S + {\rm d}S$, which is given by

$$P(S,\omega)\,{\rm d}S = \frac{1}{\sqrt{2\pi}}\frac{\omega}{S^{3/2}}\exp\left(-\frac{\omega^2}{2S}\right){\rm d}S \tag{5}$$

(Bond et al. 1991; Bower 1991; LC93). After conversion to number counting, this probability function yields the PS mass function of equation (2).

[1] Here $D(z)$ corresponds to the linear growth factor normalized to unity at the present.

Since for random walks the upcrossing probabilities are independent of the path taken (i.e. the upcrossing is a Markov process), the probability for a change ΔS in a time-step $\Delta\omega$ is simply given by equation (5) with S and ω replaced with ΔS and $\Delta\omega$, respectively. This allows one immediately to write down the *conditional* probability that a particle in a halo of mass M_2 at z_2 was embedded in a halo of mass M_1 at z_1 (with $z_1 > z_2$) as

$$P(S_1,\omega_1|S_2,\omega_2)\,\mathrm{d}S_1 = \frac{1}{\sqrt{2\pi}}\frac{(\omega_1-\omega_2)}{(S_1-S_2)^{3/2}}\exp\left[-\frac{(\omega_1-\omega_2)^2}{2(S_1-S_2)}\right]\mathrm{d}S_1. \tag{6}$$

Converting from mass weighting to number weighting, one obtains the average number of progenitors at z_1 in the mass interval M_1, $M_1+\mathrm{d}M_1$ which by redshift z_2 have merged to form a halo of mass M_2:

$$\frac{\mathrm{d}N}{\mathrm{d}M_1}(M_1,z_1|M_2,z_2)\,\mathrm{d}M_1 = \frac{M_2}{M_1}P(S_1,\omega_1|S_2,\omega_2)\left|\frac{\mathrm{d}S}{\mathrm{dM}}\right|\mathrm{d}M_1. \tag{7}$$

3 CONSTRUCTING MASS ACCRETION HISTORIES

Using the EPS conditional probabilities for halo progenitor masses, one can construct detailed histories of the mass assembly of dark matter haloes. Here we are interested in computing the 'mass accretion histories' (hereafter MAHs) of dark matter haloes, which we define as $\Psi(M_0,z)\equiv M(z)/M_0$. Here $M(z)$ is defined as the mass of the 'main progenitor halo', and M_0 is the halo mass at $z=0$.

When tracing back in time, each halo breaks up into a number of progenitor haloes, which themselves break up into progenitors, etc. Given this complicated history of the mass evolution of a halo (often referred to as the 'merger tree'), we need to define what we actually mean by the 'main progenitor' at an earlier time. We follow previous studies (LC93; Eisenstein & Loeb 1996; Nusser & Sheth 1999) and define $M(z)$ as the main trunk of the merger tree, i.e. at each time-step we associate $M(z)$ with the mass of the most massive progenitor (hereafter MMP), and we follow that progenitor, and that progenitor only, further back in time. This way the main progenitor halo never actually accretes other haloes that are more massive than itself. Note that, although at each branching point we follow the most massive branch, this does not necessarily imply that the main progenitor is also the most massive of *all* progenitors at a given redshift.

In what follows we use M_0 to denote the present-day mass of a halo. At each individual time-step we use M to refer to the parent mass for which we seek the most massive progenitor a time-step $\Delta\omega$ earlier, and we use M_p to indicate the mass of a progenitor halo.

3.1 Previous methods

In an infinitesimally small time-interval $\Delta\omega$ a change ΔS results from a *single* merger. Therefore, an approximate method for constructing MAHs is to consider small time-steps, and to assume that the change in mass associated with that finite time-interval reflects a single merger event. In that case, the MMP has a mass $M_\mathrm{p}\geq M/2$ and the construction of MAHs becomes very simple: at each time-step one draws a single ΔS from the probability distribution

$$P(\Delta S,\Delta\omega)\,\mathrm{d}\Delta S = \frac{1}{\sqrt{2\pi}}\frac{\Delta\omega}{\Delta S^{3/2}}\exp\left[-\frac{(\Delta\omega^2)}{2\Delta S}\right]\mathrm{d}\Delta S, \tag{8}$$

and one defines the mass of the main progenitor as $\max(M_\mathrm{p},\ M-M_\mathrm{p})$, where $\sigma^2(M_\mathrm{p})=\sigma^2(M)+\Delta S$. An alternative approach which leads to almost the same results is to accept only values of ΔS in the range $[0,\ \sigma^2(M/2)-\sigma^2(M)]$. This method, which we call the 'binary' method, was suggested by LC93, and has been used by Eisenstein & Loeb (1996) to compute the minimum intrinsic scatter in the Tully–Fisher relation. However, as already pointed out by LC93, this method leads to some inconsistencies regarding halo formation times, the reason for which is easily understood. The number density of progenitor masses diverges at small mass [a direct reflection of the fact that for CDM $\sigma^2(M)\rightarrow\infty$ when $M\rightarrow 0$], and the assumption of a single merger event breaks down dramatically for finite time-steps, even when chosen to be very small. In other words, there is a finite, non-negligible, probability that the mass of the MMP is less than $M/2$. This introduces, at each time-step, a systematic bias towards a main progenitor that is too massive, resulting in formation redshifts that are too high.

An alternative method for constructing MAHs was suggested by Nusser & Sheth (1999), who drew the progenitor mass from the *number*-weighted distribution function (equation 7) with $M/2\leq M_\mathrm{p}\leq M$. Although, as they show, this leads to better consistency with halo formation times, this method suffers from a similar shortcoming as again the assumption is made that the MMP is always more massive than $M/2$. However, this is only formally true in the limit $\Delta\omega\rightarrow 0$, for which the integral of $\mathrm{d}N/\mathrm{d}M_1$ (equation 7) from $M/2$ to M becomes unity (i.e. it is certain that the MMP is more massive than $M/2$).

3.2 An improved method

The discussion above suggests that, in order to construct MAHs using finite time-steps, one has to drop the assumption of single merger events. This implies that at each time-step one needs to construct a complete set of halo masses M_i that are to be considered the progenitor haloes that a time-step $\Delta\omega$ later have merged to form the parent halo with mass M. An important constraint on the set M_i is that $\sum M_i = M$, i.e. the total mass needs to be conserved at each time-step. The MAH is then easily constructed by picking the most massive of M_i, and repeating the same procedure stepping back in time until the mass of the main progenitor is as small as desired.

Unfortunately, the construction of sets of progenitors is not a trivial matter. In addition to conserving mass at each time-step, a successful merger tree also has to satisfy the requirement that, at each time-step, the distribution of the number of progenitors as a function of mass is consistent with equation (7). However, since the number of haloes diverges at very small masses, one must impose a minimum halo mass. Progenitors with masses below this threshold are not considered as individual haloes, but their mass is assumed to accrete smoothly on to the parent halo. As was previously pointed out by Somerville & Kolatt (1999, hereafter SK99), there seems to be no algorithm for drawing sets of progenitor masses that satisfies both constraints simultaneously. Kauffmann & White (1993) circumvented this problem by reproducing the progenitor mass distribution exactly, but by only enforcing mass conservation approximately. Here we follow the scheme of SK99, which conserves mass exactly while only approximately reproducing the progenitor mass distribution. This method, termed the N-branch method with accretion, has been shown to yield results in good agreement with numerical simulations (Somerville et al. 2000). Here we briefly summarize the method and we refer the interested

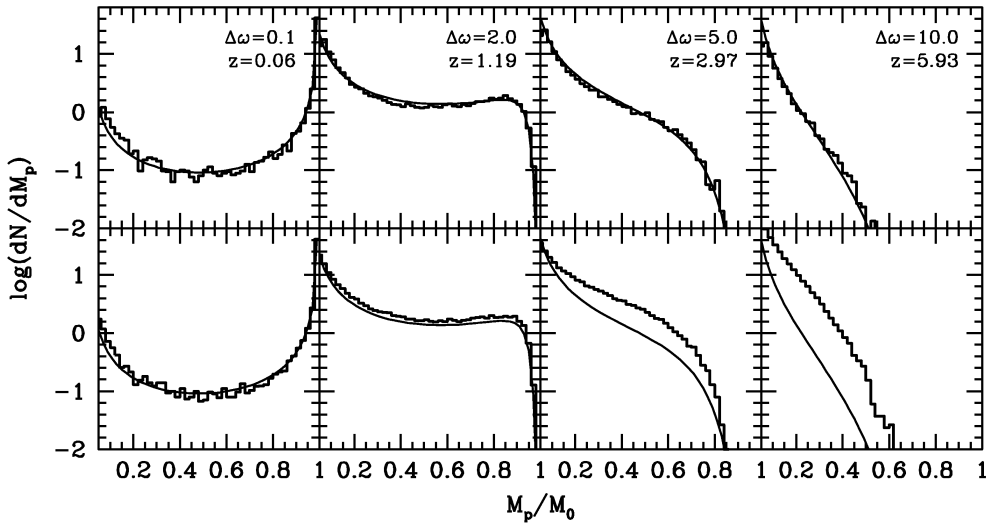

Figure 1. Mass functions of progenitors (by number) for a halo with present-day mass $M_0 = 10^{12}\,h^{-1}\,\mathrm{M}_\odot$ in an EdS universe with $h = 0.65$ and $\sigma_8 = 1.0$. Histograms correspond to the average number of progenitors found in 15 000 random realizations of the merger tree. Only progenitors more massive than 5 per cent of the parent are considered (i.e. $M_{\rm min} = 0.05M$, see text), and we therefore only plot results for $M_{\rm p}/M_0 > 0.05$. The solid lines correspond to the EPS prediction given by equation (7). Results are shown for four 'output' times of the merger trees, the corresponding $\Delta\omega$ and redshift of which are indicated. In the upper panels results are shown for merger trees that are constructed using a fixed time-step of $\Delta\omega = 0.1$. This results in progenitor numbers in excellent agreement with the direct EPS prediction. In the lower panels, progenitor masses are computed using a single time-step (with $\Delta\omega$ as indicated in the upper panels). In this case, too many progenitors are found compared with the EPS prediction. This indicates that, for the merger tree to yield self-consistent results, sufficiently small time-steps have to be used.

reader to SK99 for more details (as well as for a detailed discussion on other, less successful, methods for constructing merger trees).

The method of SK99 is based on drawing halo masses from the mass-weighted probability function (8). With each new halo drawn it is checked whether the sum of the progenitor masses exceeds the mass of the parent M. If this is the case the halo is rejected and a new progenitor mass is drawn. Any progenitor with $M_{\rm p} < M_{\rm min}$ is added to the mass component $M_{\rm acc}$ that is considered to be accreted on to the parent in a smooth fashion (i.e. the formation history of these small mass progenitors is not followed further back in time). Here $M_{\rm min}$ is a free parameter that has to be chosen to be sufficiently small. This procedure is repeated until the total mass left ($M - M_{\rm acc} - \sum M_{\rm p}$) is less than $M_{\rm min}$. This remaining mass is assigned to $M_{\rm acc}$ and one moves on to the next time-step.

In principle, since the upcrossing of trajectories through a boundary is a Markov process, the statistics of progenitor masses should be independent of the time-steps taken. However, the SK99 algorithm is based on the *single* halo probability (equation 8), which does not contain any information about the *set* of progenitors that make up the mass of M (mass conservation is enforced 'by hand', by rejecting progenitor masses that overflow the mass budget). Therefore it is not clear whether the results are time-step-independent, and this has to be tested. In the upper panels of Fig. 1 we plot the number distribution of progenitor masses at various redshifts obtained using the SK99 scheme with a fixed time-step of $\Delta\omega = 0.1$. Results are plotted for a halo with $M_0 = 10^{12}\,h^{-1}\,\mathrm{M}_\odot$ in an Einstein–de Sitter (EdS) universe with $\Omega_0 = 1$, $\Omega_\Lambda = 0$, $\sigma_8 = 1.0$ and $h = 0.65$. Histograms correspond to the distributions obtained from 15 000 random realizations of the merger tree, with $M_{\rm min} = 0.05M$. Solid lines correspond to the EPS prediction of equation (7). In the lower panels we show the same results, except that we have now computed the progenitor masses in a *single* time-step (as indicated in the upper panels): i.e. in the panels on the right, the upper panel shows the results when using 100 time-steps of $\Delta\omega = 0.1$, each time computing the progenitors of all previous progenitors, etc. The lower panel, on the other hand, show the results when computing the progenitors using a single time-step of $\Delta\omega = 10.0$. As can be seen, when using small enough time-steps the number density of progenitor masses is in excellent agreement with equation (7). However, when too large time-steps are used, the method over-predicts the number of progenitors quite dramatically. We thus conclude, confirming the results of SK99, that as long as small enough time-steps are used, the algorithm outlined above provides an accurate method for constructing merger trees.

Based on this scheme we use the following algorithm to construct MAHs:

(1) choose a present-day halo mass M_0 and set $M = M_0$ and $z = 0$;

(2) set $M_{\rm left} = M$ and compute the progenitor redshift $z_{\rm p}$ from $\Delta\omega = \delta_{\rm c}(z_{\rm p}) - \delta_{\rm c}(z)$;

(3) draw ΔS from the probability distribution (8) and compute the corresponding progenitor mass $M_{\rm p}$ from $\sigma^2(M_{\rm p}) = \sigma^2(M) + \Delta S$;

(4) if $M_{\rm p} > M_{\rm left}$ the progenitor mass is too big: go to 3;

(5) set the mass of the MMP to $M_{\rm MMP} = \max[M_{\rm p}, M_{\rm MMP}]$ and the mass left in the set to $M_{\rm left} = M_{\rm left} - M_{\rm p}$;

(6) if $M_{\rm MMP} \geq M_{\rm left}$ then we have found the MMP; in that case we proceed to the next time-step: we set $M(z_{\rm p}) = M_{\rm MMP}$, $M = M_{\rm MMP}$, $z = z_{\rm p}$, and go to 2;

(7) go to 3.

This procedure is repeated until the mass of the main progenitor is as small as desired. Note that, as is evident from step (5), we do not need to construct an entire set of progenitors; we can stop once the most massive of the progenitors already drawn is larger than the mass left in the set, and we thus do not need to define a minimum progenitor mass $M_{\rm min}$. Throughout we use a fitting function for $\sigma^2(M)$ that is accurate to better than 0.5 per cent over the entire mass range $10^6 \leq M \leq 10^{16}\,h^{-1}\,\mathrm{M}_\odot$ (see Appendix A). The

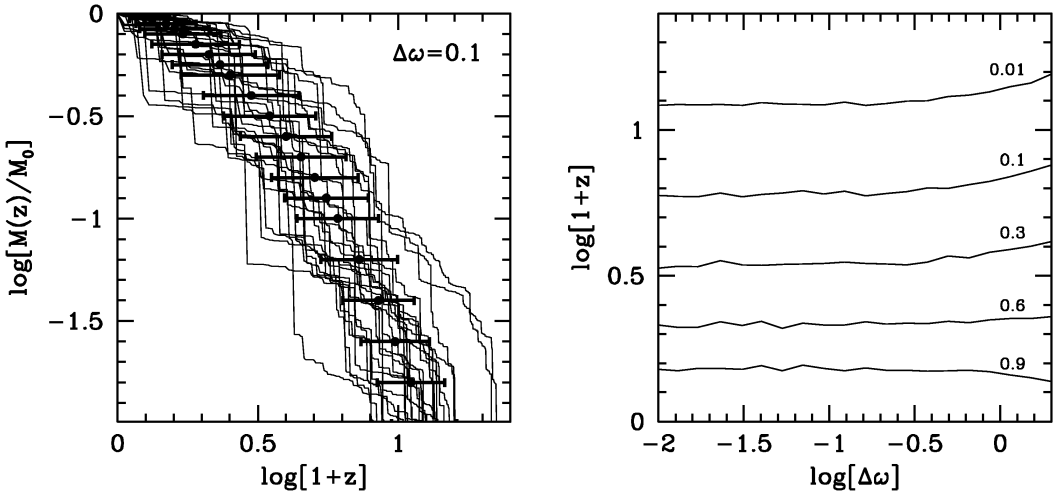

Figure 2. The panel on the left plots 25 random MAHs for a halo with $M_0 = 5.0 \times 10^{11}\, h^{-1}\, \mathrm{M}_\odot$ in an EdS universe with $h = 0.65$ and $\sigma_8 = 1.0$. The thick solid dots with error bars correspond to the average and standard deviations as determined from 1000 such realizations. A time-step of $\Delta\omega = 0.1$ is used. The panel on the right plots curves of constant $\langle\Psi\rangle$ (as indicated) as function of the time-step $\Delta\omega$ used in the construction of the MAHs. Each $\langle\Psi\rangle$ is determined from 1000 random realizations of the mass accretion history. For $\Delta\omega < 0.3$ the average MAHs converge to a robust result, while for larger time-steps $\langle\Psi\rangle$ depends on the actual value of $\Delta\omega$ used. This again suggests that a successful construction of MAHs requires a sufficiently small time-step, and we adopt $\Delta\omega = 0.1$ throughout.

power spectrum $P(k)$ is characterized by the shape parameter Γ. Unless stated otherwise we use the form suggested by Sugiyama (1995),

$$\Gamma = \Omega_0\, h \exp[-\Omega_{\rm b}(1 + \sqrt{2\,h}/\Omega_0)], \tag{9}$$

and we adopt a baryon mass density of $\Omega_{\rm b} = 0.019\, h^{-2}$ (Tytler et al. 1999).

We now define the *average* mass accretion history (hereafter AMAH) of a halo of mass M_0 as

$$\langle\Psi(M_0, z)\rangle = \frac{1}{N}\sum_{i=1}^{N} \Psi_i(M_0, z), \tag{10}$$

where the summation is over an ensemble of N random realizations $\Psi_i(M_0, z)$. Unless stated otherwise, we use $N = 1000$ and $\Delta\omega = 0.1$. In the left-hand panel of Fig. 2 we show an example. The thin lines are 25 random realizations for the MAH of a halo with $M_0 = 5.0 \times 10^{11}\, h^{-1}\, \mathrm{M}_\odot$ in an EdS universe with $\sigma_8 = 1.0$ and $h = 0.65$. The solid dots with errorbars correspond to the AMAH and its standard deviation (averaged over 1000 random realizations).

The right-hand panel of Fig. 2 plots the average redshifts at which $\langle\Psi\rangle = (0.01, 0.1, 0.3, 0.6, 0.9)$ as function of the time-step $\Delta\omega$. Note how only for sufficiently small time-steps ($\Delta\omega \lesssim 0.3$) are the values of $\langle\Psi\rangle$ not time-step-dependent. This reflects the problem outlined above, that if the time-step is too big, the distribution of progenitor masses is no longer consistent with the EPS prediction of equation (7). Results for other halo masses and cosmologies are similar, and we therefore adopt $\Delta\omega = 0.1$ throughout.

4 COMPARISON WITH NUMERICAL SIMULATIONS

Although the (extended) PS formalism is a valuable tool in the study of hierarchical structure formation, it is based on a number of questionable assumptions (e.g. spherical collapse). Therefore it is essential that any statistic extracted using the PS formalism is tested against numerical simulations.

4.1 Description of the simulations

In order to test our algorithm for constructing MAHs, we compare our results with the high-resolution ΛCDM simulation of the GIF project (Kauffmann et al. 1999; Diaferio et al. 2001). This simulation is performed using the parallel adaptive particle–particle particle–mesh ($\mathrm{AP^3M}$) code called HYDRA (Couchman, Thomas & Pearce 1995) and follows the evolution of 256^3 ($\sim 16.8 \times 10^6$) particles in a $141.3\, h^{-1}$ Mpc box. The cosmological parameters used are $\Omega_0 = 0.3$, $\Omega_\Lambda = 0.7$, $h = 0.7$ and $\Gamma = 0.21$. The power spectrum of density fluctuations is normalized to $\sigma_8 = 0.9$, in agreement with the observed abundance of massive clusters (Eke, Cole & Frenk 1996). The particle mass and softening length are $1.4 \times 10^{10}\, h^{-1}\, \mathrm{M}_\odot$ and $30\, h^{-1}$ kpc, respectively.

The particle positions and velocities are stored at 43 different redshifts between $z = 12$ and 0. At each output time, haloes are identified using the standard friends-of-friends (FOF) percolation algorithm (Davis et al. 1985), where a linking length of 0.2 times the mean inter-particle separation is adopted. The mass associated with each of these haloes, denoted by $M_{\rm FOF}$, is simply given by the number of particles linked together times the single particle mass.

A halo at redshift z_2 is defined as a progenitor of a halo at redshift $z_1 < z_2$ if (i) more than half of its particles are included in the halo at z_1, and (ii) its most bound particle is also included. Using lists of progenitors for all haloes and for all output times,[2] a MAH is constructed as follows. We start with a halo at $z = 0$ and identify all its progenitors at the previous time-step z_1. The new halo mass $M(z_1)$ is then simply defined as the mass of the most massive of these progenitors, and this procedure is repeated for all subsequent output times. A more detailed description of the construction of the halo merger trees from these GIF simulations can be found in Kauffmann et al. (1999).

4.2 Comparison of MAHs

Here we compare the MAHs of dark matter haloes in the

[2] Available at http://www.mpa-garching.mpg.de/GIF/

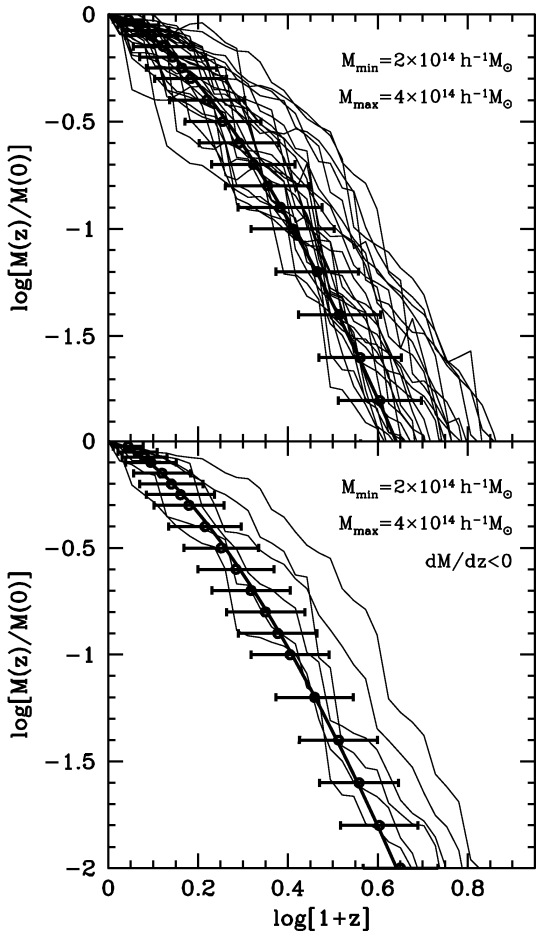

Figure 3. The thin lines represent MAHs for haloes in the ΛCDM GIF simulation. In the upper panel we plot the MAHs for 25 (randomly selected) haloes with $2.0\times10^{14} \leq M_{\rm FOF} \leq 4.0\times10^{14}\,h^{-1}\,{\rm M}_\odot$. The thick lines and dots with error bars correspond to the average MAH computed using our method based on the EPS formalism for a halo mass of $M_0 = 2.75\times10^{14}\,h^{-1}\,{\rm M}_\odot$, corresponding to the average FOF mass of the 25 haloes in the simulation. As can be seen, haloes in the simulation seem to form a little bit earlier as predicted by the EPS formalism. In the lower panel we plot the MAHs of those FOF groups in the above mass interval that have $dM/dz < 0$ at all times; only six haloes obey this criterion. As can be seen, the MAHs of these haloes are not statistically different from those in the upper panel, and are equally inconsistent with the EPS prediction (see discussion in text).

simulation with the AMAHs computed using the EPS formalism as outlined in Section 3.2.

In the upper panel of Fig. 3 we plot the MAHs for 25 (randomly selected) haloes in the simulation which at $z = 0$ have masses in the range $2.0\times10^{14} \leq M_{\rm FOF} \leq 4.0\times10^{14}\,h^{-1}\,{\rm M}_\odot$. This mass range is chosen to ensure haloes with large numbers of particles, so that we are less sensitive to resolution issues. We only accept haloes for which the MAHs can be traced back to the point where $\Psi \leq 0.01$ (i.e. in some cases no progenitors can be identified in the simulation before the mass of the main progenitor has fallen below 1 per cent of the present-day mass). The thick solid dots with error bars correspond to the AMAH computed using the EPS formalism (for exactly the same cosmological parameters as used in the simulation) for a halo with $M_0 = 2.75\times10^{14}\,h^{-1}\,{\rm M}_\odot$ which corresponds to the average mass of the 25 haloes in the simulation. Although the overall shape of the MAHs and the amounts of scatter are fairly similar, the MAHs of the haloes in the numerical simulation are systematically offset to higher redshifts (i.e. the haloes in the simulation seem, on average, to form somewhat earlier).

One possible explanation for this inconsistency is that the haloes in the simulation often have progenitors that are more massive than the parent. This can have several causes. Haloes in the simulations are susceptible to tidal stripping, which can cause the mass of the main progenitor actually to *decrease* with time. In addition, during a (high velocity) encounter two haloes may temporarily be linked together by the FOF algorithm, which causes $M(z)$ to increase and subsequently decrease again. These effects are not modelled by the EPS formalism, which only allows halo masses to grow with time. We can investigate the effect that this has on the statistics of our MAHs by only selecting haloes from the simulation that, at each time-step, have $dM/dz < 0$. Only six of the 35 haloes in our mass interval obey this criterion, and their MAHs are plotted in the lower panel of Fig. 3. Although the number statistics are poor, it is evident that these MAHs are not statistically different from those that occasionally show $dM/dz > 0$, and they show a similar inconsistency with respect to the expected AMAH. We thus conclude that the inconsistencies between the MAHs from the simulations and those from the EPS formalism are not related to the fact that the latter does not take possible mass loss into account. A more likely cause for the inconsistency is discussed in Section 4.4.

4.3 Comparison of halo formation times

Another useful statistic for comparison is the distribution of halo formation redshifts. We use the definition of LC93 and define the halo formation redshift, $z_{\rm f}$, as the redshift at which $\Psi = 0.5$, i.e. at which the mass of the main progenitor is half the present-day mass.

LC93 presented two methods for computing the distribution of formation times. The first is based on the number-weighted mass distribution of progenitor haloes (equation 7). As argued by LC93, integrating this equation from $M_0/2$ to M_0 gives the probability that the progenitor mass is more massive than $M_0/2$, which is equal to the probability that the halo formation time was earlier than this. Upon defining the scaled variables

$$\tilde{S} = \frac{\sigma^2(M) - \sigma^2(M_0)}{\sigma^2(M_0/2) - \sigma^2(M_0)} \tag{11}$$

and

$$\tilde{\omega}_{\rm f} = \frac{\delta_{\rm c}(z_{\rm f}) - \delta_{\rm c}(0)}{\sqrt{\sigma^2(M_0/2) - \sigma^2(M_0)}}, \tag{12}$$

one can write the probability distribution for halo formation times as

$$P(\tilde{\omega}_{\rm f}) = \frac{1}{\sqrt{2\pi}} \int_0^1 \frac{M_0}{M} \left(\frac{\tilde{\omega}_{\rm f}^2}{\tilde{S}^{5/2}} - \frac{1}{\tilde{S}^{3/2}} \right) \exp\left(-\frac{\tilde{\omega}_{\rm f}^2}{2\tilde{S}} \right) {\rm d}\tilde{S}, \tag{13}$$

where M is solved from equation (11). The advantage of using the variables $\tilde{S}$ and $\tilde{\omega}_{\rm f}$ is that $P(\tilde{\omega}_{\rm f})$ depends only very mildly on mass and cosmology (this dependence is largely absorbed by the variables themselves).

Another method for computing halo formation times is to use the actual MAHs themselves, and to identify the redshift at which the main progenitor mass equals half the present-day mass. LC93 used their 'binary' Monte Carlo method for constructing MAHs (discussed in Section 3.1), and found a distribution $P(\tilde{\omega}_{\rm f})$ that was offset from that of equation (13) to higher values of $\tilde{\omega}_{\rm f}$. Lacey

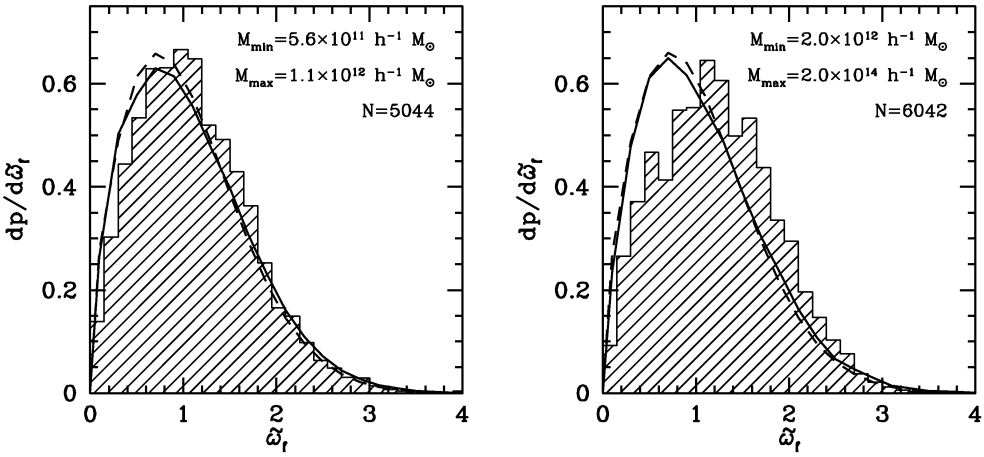

Figure 4. The hatched histograms correspond to the distribution of halo formation times (parametrized by the scaled variable $\tilde{\omega}_{\rm f}$) for haloes in the simulation (with FOF masses as indicated in the two panels). The solid lines are the distributions of $\tilde{\omega}_{\rm f}$ computed from 2×10^5 random realizations of the MAH for a halo with $M_0 = 8.4\times10^{11}\,h^{-1}\,{\rm M}_\odot$ (left-hand panel) and $M_0 = 1.1\times10^{13}\,h^{-1}\,{\rm M}_\odot$ (right-hand panel). These masses correspond to the average halo masses in the two simulation samples. Dashed lines correspond to $P(\tilde{\omega}_{\rm f})$ of equation (13) for the same masses, and are in excellent agreement with the distributions obtained directly from the MAHs. However, the formation times in the simulation are offset from those of the EPS formalism, whereby the discrepancy is larger for more massive haloes.

& Cole (1994) determined the distributions of halo formation times of dark matter haloes in simulations with scale-free power spectra, and found them to be in excellent agreement with the analytical prediction of equation (13), but inconsistent with $P(\tilde{\omega}_{\rm f})$ derived using the Monte Carlo method. As indicated in Section 3.1, the 'binary' Monte Carlo method used by LC93 is based on the false premise that the most massive progenitor has mass $M_{\rm p} > M/2$, which leads to a systematic offset of halo formation redshifts to too high values.

We now re-examine the issue of halo formation times using the high-resolution ΛCDM simulation and our improved method for constructing MAHs. In order to improve accuracy we use linear interpolation between the time-steps that bracket $\Psi = 0.5$ (for the haloes in the simulations as well as for the MAHs constructed using the EPS formalism). We convert $z_{\rm f}$ to the scaled variable $\tilde{\omega}_{\rm f}$, so that $P(\tilde{\omega}_{\rm f})$ depends only very weakly on cosmology and halo mass. This allows us to compare distributions of $\tilde{\omega}_{\rm f}$ for relatively large mass intervals, providing better statistics.

We compute the distribution of $\tilde{\omega}_{\rm f}$ for two samples of haloes. The first consists of 5044 haloes with present-day masses $5.6\times10^{11} \leq M_{\rm FOF} \leq 1.12\times10^{12}\,h^{-1}\,{\rm M}_\odot$). This mass range corresponds to haloes that, at $z = 0$, consist of between 40 and 80 particles. The resulting distribution of $\tilde{\omega}_{\rm f}$ is indicated by the hatched histogram in the left-hand panel of Fig. 4. The solid curve corresponds to the distribution of $\tilde{\omega}_{\rm f}$ derived from 2×10^5 MAHs for a halo with $M_0 = 8.4\times10^{11}\,h^{-1}\,{\rm M}_\odot$ (corresponding to the average mass of the 5044 haloes in the simulation), using the same cosmological parameters as in the simulation. The two distributions are in good agreement, although the mean for the simulated haloes is slightly offset to higher $\tilde{\omega}_{\rm f}$. The dashed curve corresponds to $P(\tilde{\omega}_{\rm f})$ of equation (13), also for a mass of $8.4\times10^{11}\,h^{-1}\,{\rm M}_\odot$. This distribution is in excellent agreement with that derived using the MAHs. This shows that our method for constructing MAHs is, within the EPS framework, self-consistent, and does not suffer from the inconsistencies found when using the LC93 'binary' method.

The right-hand panel of Fig. 4 plots similar results but now for the 6042 haloes in the mass range $2.0\times10^{12} \leq M_{\rm FOF} \leq 4.0\times10^{12}\,h^{-1}\,{\rm M}_\odot$. The agreement with the MAHs is somewhat poorer as in the case of the lower mass range, with significantly higher formation redshifts for the haloes in the simulation. This is, of course, another manifestation of the inconsistencies found between the MAHs in the simulations and those computed using the EPS formalism (cf. Fig. 3).

4.4 Ellipsoidal collapse

In addition to the inconsistencies with the MAHs indicated above, various studies in the past have pointed out that the standard, unconditional PS mass function (equation 2) over- (under-) predicts the number of low- (high-) mass haloes when compared with numerical simulations (e.g. Jain & Bertschinger 1994; Tormen 1998; Gross et al. 1998; Governato et al. 1999). This is generally interpreted as a consequence of the assumption of spherical collapse, and numerous studies have shown that considering ellipsoidal rather than spherical collapse brings the PS mass function into much better agreement with simulations (e.g., Monaco 1995; Bond & Myers 1996; Audit, Teyssier & Alimi 1997; Lee & Shandarin 1998; Sheth & Tormen 1999; Lanzoni, Mamon & Guiderdoni 2000; Sheth, Mo & Tormen 2001; Jenkins et al. 2001).

We can investigate a modification of the spherical collapse model, by multiplying the critical collapse density $\delta_{\rm c}$ (as defined in Section 2) with a fudge factor a and by examining how a depends on halo mass, if at all. One of the advantages of using the scaled variable $\tilde{\omega}_{\rm f}$ is that $P(\tilde{\omega}_{\rm f})$ is independent of a, at least for the MAHs computed using the EPS formalism. In the case of the haloes in the simulation one has that $\tilde{\omega}_{\rm f} \propto a$, and one can therefore immediately re-scale the histograms in Fig. 4 to determine the best-fitting value of a. Doing so, we find $a \simeq 0.94$ and $\simeq$0.82 for the mass intervals plotted in the panels on the left ($M_0 = 8.4\times10^{11}\,h^{-1}\,{\rm M}_\odot$) and right ($M_0 = 1.1\times10^{13}\,h^{-1}\,{\rm M}_\odot$), respectively. Similarly, we find that for $a \simeq 0.8$ the AMAH plotted in Fig. 3 ($M_0 = 2.75\times10^{14}\,h^{-1}\,{\rm M}_\odot$) is in excellent agreement with the MAHs found in the simulation. Thus it seems that a modification of the spherical collapse model whereby $\delta_{\rm c}$ decreases with increasing halo mass can bring the EPS MAHs into excellent agreement with the simulations. Interestingly, as shown by Sheth et al. (2001), this is

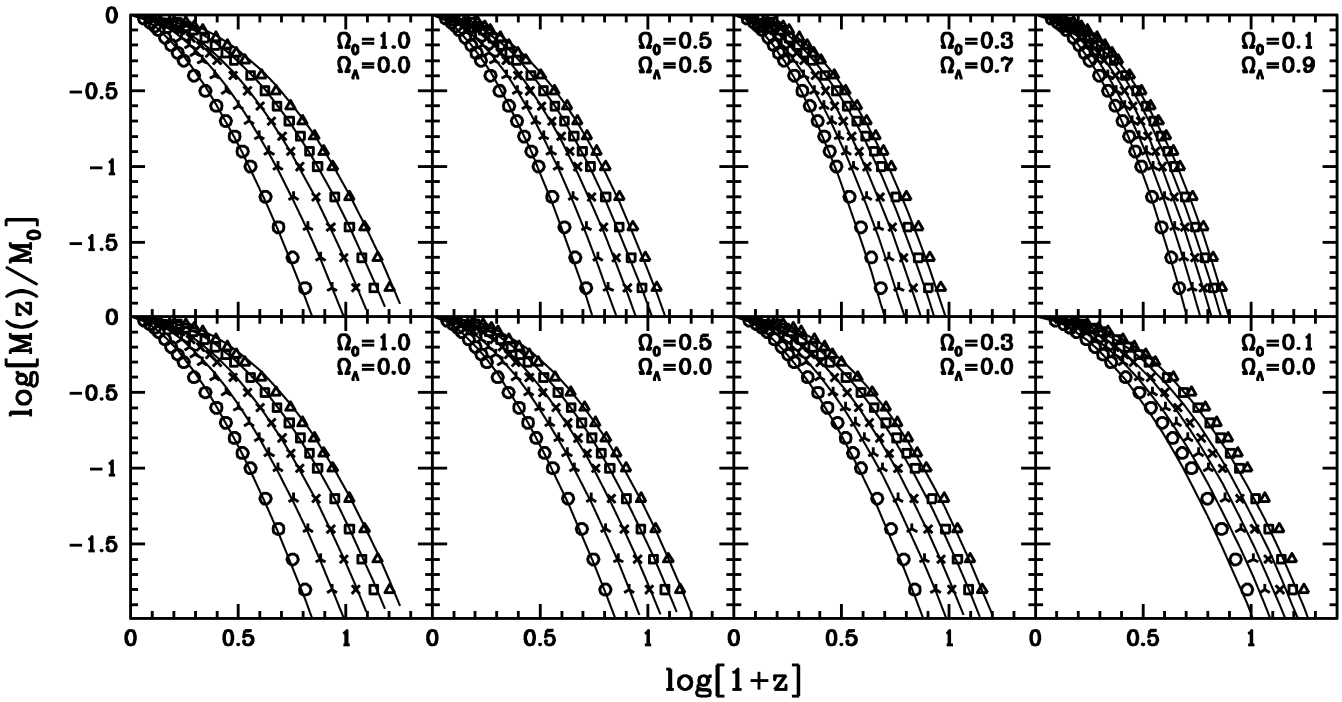

Figure 5. Average MAHs for various cosmologies (all with $\sigma_8 = 1.0$ and $h = 0.65$). Results are shown for five masses: $5.0 \times 10^9\, h^{-1}\,\mathrm{M}_\odot$ (open triangles), $5.0 \times 10^{10}\, h^{-1}\,\mathrm{M}_\odot$ (open squares), $5.0 \times 10^{11}\, h^{-1}\,\mathrm{M}_\odot$ (crosses), $5.0 \times 10^{12}\, h^{-1}\,\mathrm{M}_\odot$ (tripods) a $5.0 \times 10^{13}\, h^{-1}\,\mathrm{M}_\odot$ (open circles). Averages are determined from 10^3 random MAH realizations. Solid lines correspond to the universal MAH computed using the recipe given in Appendix A, and provide an excellent fit to the average MAHs.

exactly the kind of behaviour one expects if one takes into account that haloes are ellipsoidal rather than spherical. These authors obtain a modified critical collapse overdensity given by

$$\delta_{\rm ce}(M,z) = \delta_{\rm c}(z)\left\{1 + 0.47\left[\frac{\sigma^2(M)}{\delta_{\rm c}^2(z)}\right]^{0.615}\right\}. \qquad (14)$$

Here $\delta_{\rm c}(z)$ is the standard value for the spherical collapse model. This modification results in halo mass functions that are in excellent agreement with those found in simulations (Sheth & Tormen 1999; Jenkins et al. 2001).

Thus two separate statistics, the unconditional halo mass function and the halo formation times (i.e. the MAHs), both suggest a critical collapse density that increases with decreasing halo mass. Therefore it might be worthwhile to try to incorporate a mass-dependent critical collapse density in the EPS formalism. This requires what pundits call determining the upcrossing statistics for a *moving barrier*. However, as discussed by Sheth & Tormen (2002), no analytical expression for the conditional probability function [i.e. a moving barrier equivalent of equation (6)] is known for a barrier of the form of equation (14), and one either has to resort to an approximate fitting function, or has to use time-consuming Monte Carlo simulations to determine the upcrossing statistics. Unfortunately, as discussed in detail by Sheth & Tormen (2002), neither of these two methods is appropriate for constructing merger trees. Therefore, in what follows we adhere to the standard, spherical collapse model, but we caution the reader that, taking the numerical simulations at face value, the MAHs thus derived contain slight, mass-dependent inaccuracies.

5 A UNIVERSAL FORM FOR THE MASS ACCRETION HISTORIES

Fig. 5 plots the average MAHs for various halo masses (different symbols) and cosmologies (different panels). Upper panels correspond to ΛCDM cosmologies with $\Omega_0 + \Omega_\Lambda = 1$, while lower panels are for OCDM cosmologies without a cosmological constant (in both cases we adopt $h = 0.65$ and $\sigma_8 = 1.0$). These plots clearly show the well-known behaviour that smaller mass haloes form earlier, which is a direct reflection of the fact that $\sigma(M)$ increases with decreasing mass. The cosmology dependence of the MAHs is easily understood if one takes into account how the mass variance $\sigma(M)$ and the linear growth factor $D(z)$ depend on cosmology. On the mass scales of interest, a decrease in Ω_0 causes $\sigma(M)$ to decrease (for fixed σ_8), which implies lower formation redshifts (i.e. lower accretion rates). At the same time, a decrease in Ω_0 causes an increase in $D(z)$ (at fixed redshift), so that a time-step $\Delta\omega$ implies a larger Δz. This drives the MAHs to higher formation times. The net result of a decrease in Ω_0, therefore, depends on which of these two effects dominates. Since $\mathrm{d}\sigma/\mathrm{d}M$ decreases with Ω_0 the $\sigma(M)$ effect on $z_{\rm f}$ is stronger for less massive systems. Therefore one expects the $\sigma(M)$ effect to dominate for small enough masses, resulting in a decrease of $z_{\rm f}$. Furthermore, the increase of $D(z)$ with decreasing Ω_0 is stronger for a universe with $\Omega_\Lambda = 0$ than for one with $\Omega_\Lambda = 1 - \Omega_0$, so that the mass scale below which $z_{\rm f}$ decreases with decreasing Ω_0 is higher in an open cosmology compared with a Λ cosmology. This behaviour is nicely reproduced by the MAHs plotted in Fig. 5. In the upper panels, decreasing Ω_0 only very mildly affects the MAH of a $5 \times 10^{13}\, h^{-1}\,\mathrm{M}_\odot$ halo. For this mass the two effects mentioned above largely cancel each other. For less massive haloes the $\sigma(M)$ effect dominates, causing the haloes to form later in lower-Ω_0

cosmologies. In fact, for $\Omega_0 = 0.1$ the mass dependence of MAHs is much reduced compared with the EdS cosmology. In OCDM cosmologies, the $D(z)$ effect is relatively stronger and now it is the low-mass systems that are hardly affected, while more massive haloes increase their formation redshift with decreasing Ω_0.

After experimenting with a variety of fitting functions, we find that the AMAHs are well fitted by the following simple form:

$$\log\langle\Psi(M_0,z)\rangle = -0.301\left[\frac{\log(1+z)}{\log(1+z_{\rm f})}\right]^{\nu}, \qquad (15)$$

where $z_{\rm f}$ and ν are free fitting parameters. Note that with this definition $z_{\rm f}$ corresponds to the formation redshift as defined in Section 4.3 [i.e. $M(z_{\rm f}) = M_0/2$]. In what follows we shall refer to equation (15) as the 'universal' MAH. Recently Wechsler et al. (2001) investigated the MAHs of individual dark matter haloes in a ΛCDM simulation which they fitted with $\Psi(M_0,z) = {\rm e}^{-\alpha z}$ (with α a free fitting parameter). In Appendix B we compare this one-parameter fitting function with the universal MAH of equation (15), and we show how α may be estimated from the formation redshift $z_{\rm f}$.

In order to investigate how the scale-parameters ν and $z_{\rm f}$ depend on mass and cosmology, we proceed as follows: we randomly draw values for Ω_0, M_0 and σ_8 from the intervals $0.1 \leq \Omega_0 \leq 1.0$, $10^9 \leq M_0 \leq 10^{14}\,h^{-1}\,{\rm M}_\odot$ and $0.5 \leq \sigma_8 \leq 1.5$. For each of these models we compute the AMAH from 10^3 random realizations of the MAH, and we find the best-fitting values of ν and $z_{\rm f}$. In total we construct 50 AMAHs with $\Omega_\Lambda = 0$ and another 50 with $\Omega_\Lambda = 1 - \Omega_0$. As shown in Fig. 6, the best-fitting values of ν and $z_{\rm f}$ are strongly correlated, suggesting that a single parameter suffices to describe the average MAHs. In Appendix A we present a step-by-step recipe for computing ν and $z_{\rm f}$ as function of halo mass and cosmology directly.

The solid lines in Fig. 5 correspond to the universal MAHs with ν and $z_{\rm f}$ computed using this recipe. Only in the extreme case with $\Omega_0 = 0.1$ and $\Omega_\Lambda = 0.0$ (lower right panel) does the universal MAH fail to fit the average MAHs accurately. In all other cases, the universal MAH is in excellent agreement with average MAHs obtained using the method described in Section 3.2.

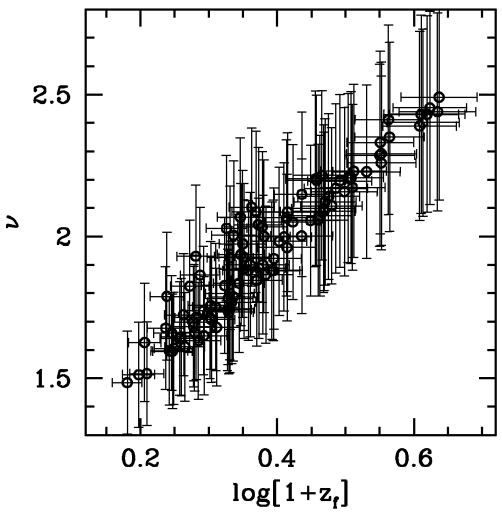

Figure 6. The correlation between the best-fitting values of the scale-parameters ν and $z_{\rm f}$ of the universal MAH, obtained by fitting equation (15) to the AMAHs of dark matter haloes with a large range of masses and for a wide variety of cosmologies. Error bars correspond to the formal errors returned by the fitting routine used. Note that ν and $\log(1+z_{\rm f})$ are strongly correlated, suggesting that a single parameter suffices to describe the average MAH of a dark matter halo (see Appendix A).

6 APPLICATION: THE ACCRETION RATE OF DARK MATTER HALOES

Using the universal MAH, the average rate at which haloes of mass M_0 accrete mass can be written as

$$\frac{{\rm d}M}{{\rm d}t}(z) = M_0\frac{{\rm d}\Psi}{{\rm d}t}(M_0,z). \qquad (16)$$

We can use this to compute the total comoving dark matter accretion rate of all haloes that at $z = 0$ have masses between M_1 and M_2, by weighting each halo by the present-day, comoving *number* density $n(M, z = 0)$:

$$\frac{{\rm d}\rho}{{\rm d}t}(z;M_1,M_2) = \int_{M_1}^{M_2}\frac{{\rm d}\Psi}{{\rm d}t}(M,z)\frac{{\rm d}n}{{\rm d}\ln M}(M,z=0)\,{\rm d}M. \qquad (17)$$

Here $\rho(z)$ is defined as the comoving mass density at redshift z of all main progenitor haloes that by $z = 0$ have evolved to become haloes with $M_1 \leq M_0 \leq M_2$. Using the universal MAH of equation (15) and the PS mass function of equation (2), this integral is easily computed numerically.

If we make the simplifying assumption that all baryons inside haloes with present-day masses in the interval $M_1 \leq M_0 \leq M_2$ were instantaneously turned into stars the moment they were accreted, multiplying equation (17) with the universal baryon fraction $f_{\rm bar}$ gives the comoving star formation rate ${\rm d}\rho_*/{\rm d}t$ as function of redshift. For $M_0 \gtrsim 10^{13}\,h^{-1}\,{\rm M}_\odot$ the cooling time is longer than the Hubble time, and such systems are therefore not expected to contribute significantly to the cosmic star formation rate. Haloes with $M_0 \lesssim 10^{10}\,h^{-1}\,{\rm M}_\odot$ have virial velocities $V_{\rm vir} \lesssim 30\,{\rm km\,s^{-1}}$, and a typical background ultraviolet radiation field can prevent the gas from cooling (e.g. Babul & Rees 1992; Kepner, Babul & Spergel 1997). Therefore it is to be expected that most star formation occurs in haloes in this mass range. We therefore set $M_1 = 10^{10}\,h^{-1}\,{\rm M}_\odot$ and $M_2 = 10^{13}\,h^{-1}\,{\rm M}_\odot$, and compute ${\rm d}\rho_*/{\rm d}t$ using $f_{\rm bar} = 0.019\Omega_0^{-1}\,h^{-2}$ (Tytler et al. 1999).

The results are shown in Fig. 7 for three different cosmologies, all with $h = 0.65$ and $\sigma_8 = 1.0$ (solid lines). The short-dashed, dotted and long-dashed curves plot the separate contributions from the mass ranges $10 \leq \log(M_0) \leq 11$, $11 \leq \log(M_0) \leq 12$ and $12 \leq \log(M_0) \leq 13$, respectively. In all three cosmologies ${\rm d}\rho_*/{\rm d}t$ increases rapidly at low redshift, peaks in the redshift interval $1 \lesssim z \lesssim 3$, and then declines (the steepness of the decline depends on cosmology). This is in good agreement with observations of the cosmic star formation rate, which increases by over an order of magnitude from $z = 0$ to 1, and which seems to peak at $1 \lesssim z \lesssim 2$ (e.g. Lilly et al. 1996; Madau et al. 1996; Steidel et al. 1996; and references therein). Clearly our assumption of instantaneous star formation with 100 per cent efficiency is a severe over-simplification. In reality, there will be a delay between accretion and star formation set by the cooling and free-fall time-scales of the halo. In addition, not all baryons take part in star formation, as present-day gas mass fractions in galaxies are clearly not zero. Furthermore, various processes can temporarily quench or enhance star formation compared with the cooling rate, and feedback processes can cause baryons to cycle through multiple star formation episodes. A more elaborate comparison with the observed cosmic star formation rate will have to take all these effects into account. Nevertheless, it is reassuring that our over-simplified

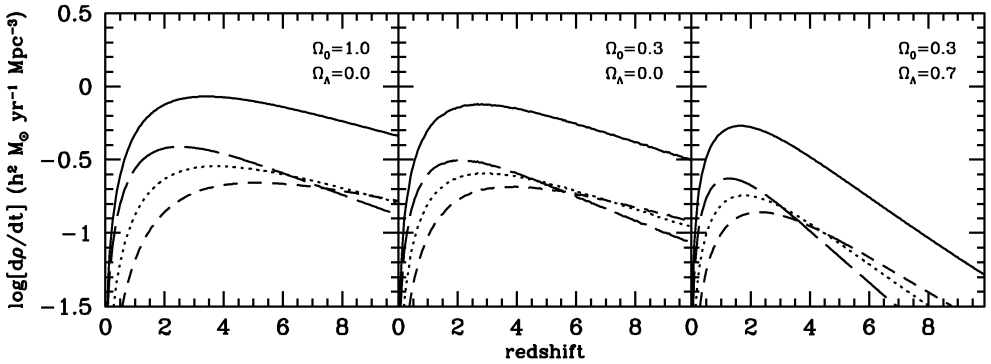

Figure 7. The baryonic mass accretion rates defined by equation (17) multiplied with the universal baryon fraction $f_{\rm bar}$. Solid lines correspond to the comoving accretion rates integrated over all haloes with present-day masses $10^{10} \leq M_0 \leq 10^{13}\,h^{-1}\,{\rm M}_\odot$. In addition we plot the contribution to these curves from three separate mass intervals: $10^{10} \leq M_0 \leq 10^{11}\,h^{-1}\,{\rm M}_\odot$ (short-dashed lines), $10^{11} \leq M_0 \leq 10^{12}\,h^{-1}\,{\rm M}_\odot$ (dotted lines) and $10^{12} \leq M_0 \leq 10^{13}\,h^{-1}\,{\rm M}_\odot$ (long-dashed lines). Results are shown for three different cosmologies as indicated (all with $h = 0.65$ and $\sigma_8 = 1.0$). The rapid increase at low z to a maximum accretion rate at $z \simeq 2$ is in good agreement with observations of the cosmic star formation history (see discussion in text).

assumptions already yield results that reproduce the main characteristics observed. This suggests that indeed the baryonic mass accretion rate is the main driving force for the cosmic star formation history, and that the universal MAH derived here may prove a useful tool in modelling the history of star formation in the Universe.

7 CONCLUSIONS

We have presented an improved method for determining the mass accretion histories (MAHs) of dark matter haloes, based on the *N*-branch merger-tree construction algorithm of Somerville & Kolatt (1999). As we have shown, this yields MAHs with formation times that are in excellent agreement with direct estimates based on the extended Press–Schechter (PS) formalism. This solves an inconsistency that hampered previous methods for constructing MAHs, which were based on a binary method where the assumption was made that the most massive progenitor is always more massive than half the mass of the parent. This, however, is a poor assumption and results in halo formation redshifts that are too high.

The MAHs and halo formation times obtained using our improved method are in reasonable agreement with high-resolution numerical simulations. The small discrepancies found seem to be larger for more massive haloes. Such mass dependence is also found when comparing the PS mass function with simulations. Various authors have suggested that this mass function discrepancy can be solved by adopting an ellipsoidal collapse model, rather than the spherical collapse model used in the standard PS formalism. Interestingly, under ellipsoidal collapse one predicts the critical collapse density to be higher for less massive systems, which is consistent with our mass dependence of the halo formation time discrepancies found.

We have shown that the average MAHs of dark matter haloes have a universal functional form. The dependence of mass and cosmology is absorbed by two parameters that can be computed accurately using simple fitting functions. Together with the universal density profile of cold dark matter (CDM) haloes (Navarro et al. 1997), and the universal angular momentum distribution of CDM haloes (Bullock et al. 2001), this universal MAH provides a complete set of simple equations that can be used to model the structure and formation of the population of dark matter haloes. The universal MAH is especially useful in modelling the formation of disc galaxies, where the detailed effects of merging are not important [e.g. the models of Firmani & Avila-Reese (2000) and van den Bosch (2001, 2002)]. In addition, the universal MAH allows a straightforward computation of the mass accretion rate of dark matter haloes, which is expected to drive the cosmic star formation rate, and allows a fast but accurate investigation of mass and/or cosmology dependences without the need for constructing ensembles of actual MAHs.

ACKNOWLEDGMENTS

I am grateful to Anthony Brown, Guinevere Kauffmann, Houjun Mo, Adi Nusser, Joel Primack, Rachel Somerville, Risa Wechsler and Simon White for useful discussions, and to the anonymous referee for helpful comments.

REFERENCES

Audit E., Teyssier R., Alimi J.-M., 1997, A&A, 325, 439
Babul A., Rees M. J., 1992, MNRAS, 255, 346
Bardeen J. M., Bond J. R., Kaiser N., Szalay A., 1986, ApJ, 304, 15
Bond J. R., Myers S., 1996, ApJS, 103, 1
Bond J. R., Cole S., Efstathiou G., Kaiser N., 1991, ApJ, 379, 440
Bower R., 1991, MNRAS, 248, 332
Bullock J. S., Dekel A., Kolatt T. S., Kravtsov A. V., Klypin A. A., Porciani C., Primack J. R., 2001, ApJ, 555, 240
Carlberg R. G., Couchman H. M. P., 1989, ApJ, 340, 47
Cole S., Kaiser N., 1988, MNRAS, 233, 637
Cole S., Aragón-Salamanca A., Frenk C. S., Navarro J. F., Zepf S. E., 1994, MNRAS, 271, 781
Cole S., Lacey C. G., Baugh C. M., Frenk C. S., 2000, MNRAS, 319, 168
Couchman H. M. P., Thomas P. A., Pearce F. R., 1995, ApJ, 452, 797
Davis M., Efstathiou G., Frenk C. S., White S. D. M., 1985, ApJ, 292, 371
Diaferio A., Kauffmann G., Balogh M. L., White S. D. M., Schade D., Ellingson E., 2001, MNRAS, 323, 999
Efstathiou G., Frenk C. S., White S. D. M., Davis M., 1988, MNRAS, 235, 715
Eisenstein D. J., Loeb A., 1996, MNRAS, 459, 432
Eke V. R., Cole S., Frenk C. S., 1996, MNRAS, 282, 263
Firmani C., Avila-Reese V., 2000, MNRAS, 315, 457
Gelb J. M., Bertschinger E., 1994, ApJ, 436, 467
Governato F., Babul A., Quinn T., Tozzi P., Baugh C. M., Katz N., Lake G., 1999, MNRAS, 307, 949
Gross M. A. K., Somerville R. S., Primack J. R., Holtzman J., Klypin A. A., 1998, MNRAS, 301, 81

Gunn J. E., Gott J. R., 1972, ApJ, 176, 1
Jain B., Bertschinger E., 1994, ApJ, 431, 495
Jenkins A., Frenk C. S., White S. D. M., Colberg J. M., Cole S., Evrard A. E., Couchman H. M. P., Yoshida N., 2001, MNRAS, 321, 372
Kauffmann G., White S. D. M., 1993, MNRAS, 261, 921
Kauffmann G., White S. D. M., Guiderdoni B., 1993, MNRAS, 264, 201
Kauffmann G., Colberg J. M., Diaferio A., White S. D. M., 1999, MNRAS, 303, 188
Kepner J. V., Babul A., Spergel D. N., 1997, ApJ, 487, 61
Lacey C., Cole S., 1993, MNRAS, 262, 627 (LC93)
Lacey C., Cole S., 1994, MNRAS, 271, 676
Lanzoni B., Mamon G. A., Guiderdoni B., 2000, MNRAS, 312, 781
Lee J., Shandarin S., 1998, ApJ, 500, 14
Lilly S. J., Le Févre O., Hammer F., Crampton D., 1996, ApJ, 460, L1
Ma C., 1996, ApJ, 471, 13
Madau P., Ferguson H. C., Dickinson M. E., Giavalisco M., Steidel C. C., Fruchter A., 1996, MNRAS, 283, 1388
Monaco P., 1995, ApJ, 447, 23
Navarro J. F., Frenk C. S., White S. D. M., 1997, ApJ, 490, 493
Nusser A., Sheth R. K., 1999, MNRAS, 303, 685
Peebles P. J. E., 1980, The Large-Scale Structure of the Universe. Princeton Univ. Press, Princeton, NJ
Press W., Schechter P., 1974, ApJ, 187, 425
Sheth R. K., Lemson G., 1999, MNRAS, 305, 946
Sheth R. K., Tormen G., 1999, MNRAS, 308, 119
Sheth R. K., Tormen G., 2002, MNRAS, 329, 61
Sheth R. K., Mo H. J., Tormen G., 2001, MNRAS, 323, 1
Somerville R. S., Kolatt T. S., 1999, MNRAS, 305, 1 (SK99)
Somerville R. S., Primack J. R., 1999, MNRAS, 310, 1087
Somerville R. S., Lemson G., Kolatt T. S., Dekel A., 2000, MNRAS, 316, 479
Steidel C. C., Giavalisco M., Pettini M., Dickinson M., Adelberger K. L., 1996, ApJ, 462, L17
Sugiyama N., 1995, ApJS, 100, 281
Tormen G., 1998, MNRAS, 297, 648
Tytler D., Burles S., Lu L., Fan X.-M., Wolfe A., Savage B., 1999, AJ, 117, 63
van den Bosch F. C., 2001, MNRAS, 327, 1334
van den Bosch F. C., 2002, MNRAS, submitted
Wechsler R. H., Bullock J. S., Primack J. R., Kravtsov A. V., Dekel A., 2001, preprint (astro-ph/0108151) (WBPKD)

APPENDIX A: A RECIPE FOR COMPUTING THE AVERAGE MASS ACCRETION HISTORY OF DARK MATTER HALOES

As shown in Section 5, the average MAH of dark matter haloes is well fitted by the universal form

$$\log\langle\Psi(M_0,z)\rangle = -0.301\left[\frac{\log(1+z)}{\log(1+z_{\rm f})}\right]^{\nu}, \qquad \text{(A1)}$$

with $z_{\rm f}$ and ν two scale-parameters that depend on halo mass and cosmology, and which are strongly correlated (cf. Fig. 6).

In order to compute $z_{\rm f}$ directly from EPS theory, we consider the cumulative probability distribution of *single-trajectory* formation redshifts given by LC93:

$$\mathrm{P}(z>z_{\rm f}|M_0) = \mathrm{erfc}\left\{\frac{\delta_{\rm c}(z_{\rm f})-\delta_{\rm c}(0)}{\sqrt{2[\sigma^2(fM_0)-\sigma^2(M_0)]}}\right\}, \qquad \text{(A2)}$$

with $\mathrm{erfc}(x)$ the complementary error function and $f=0.5$. Here $\delta_{\rm c}(z)=\delta^0_{\rm crit}[\Omega(z)]/D(z)$ with $D(z)$ the linear growth factor normalized to unity at $z=0$ (see Peebles 1980), and $\delta^0_{\rm crit}$ is the critical threshold for spherical collapse, which is well approximated by

$$\delta^0_{\rm crit}[\Omega(z)] = 0.15(12\pi)^{2/3}\Omega(z)^p \qquad \text{(A3)}$$

with

$$p=\begin{cases}0.0185 & \text{if } \Omega_0<1 \text{ and } \Omega_\Lambda=0\\ 0.0055 & \text{if } \Omega_0+\Omega_\Lambda=1\end{cases} \qquad \text{(A4)}$$

(e.g. Navarro et al. 1997) and

$$\Omega(z)=\frac{\Omega_0(1+z)^3}{\Omega_\Lambda+(1-\Omega_0-\Omega_\Lambda)(1+z)^2+\Omega_0(1+z)^3}. \qquad \text{(A5)}$$

The median value for $z_{\rm f}$ of equation (A2) is easily obtained by solving for the root of

$$\delta_{\rm c}(z_{\rm f}) = \delta_{\rm c}(0)+0.477\sqrt{2[\sigma^2(fM_0)-\sigma^2(M_0)]}. \qquad \text{(A6)}$$

As pointed out by LC93, this is *not* the same as the median halo formation redshift, as it does not necessarily follow the main progenitor. However, since equation (A6) at least contains the proper scaling with cosmological parameters, one might hope to be able to use this simple equation to model the best-fitting values of $z_{\rm f}$ by tuning the parameter f. We find excellent agreement with the best-fitting values of $z_{\rm f}$ [determined by fitting equation (A1) to the average MAHs] for $f=0.254$ (see Fig. A1).

Motivated by the strong correlation between the best-fitting values of ν and $z_{\rm f}$, we find that the power index ν is well approximated by

$$\nu = 1.211+1.858\log(1+z_{\rm f})+0.308\Omega_\Lambda^2 - 0.032\log[M_0/(10^{11}\,h^{-1}\,\mathrm{M}_\odot)] \qquad \text{(A7)}$$

(rms error of 9.0×10^{-4}). Equations (A6) (with $f=0.254$) and (A7) give the scale-parameters $z_{\rm f}$ and ν for any halo mass and cosmology, and therefore completely specify the universal MAH (A1).

Whenever we compute $\sigma(M)$ we use the following fitting function:

$$\sigma(M)=\sigma_8\frac{f(u)}{f(u_8)}. \qquad \text{(A8)}$$

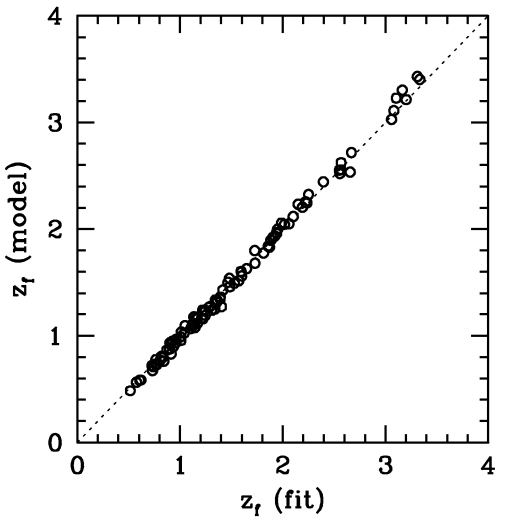

Figure A1. The values of $z_{\rm f}$ derived from equation (A6) with $f=0.254$ versus the best-fitting values of $z_{\rm f}$ determined from fitting equation (A1) to the average MAHs. Results are shown for 100 haloes that differ in both mass and cosmology (see Section 5).

Here $u_8 = 32\Gamma$ (with Γ the power spectrum shape parameter),

$$u = 3.804 \times 10^{-4} \Gamma \left(\frac{M}{\Omega_0}\right)^{1/3}, \quad \text{(A9)}$$

with M in units of $h^{-1}\,\mathrm{M}_\odot$, and

$$f(u) = 64.087(1 + 1.074u^{0.3} - 1.581u^{0.4} + 0.954u^{0.5} - 0.185u^{0.6})^{-10}. \quad \text{(A10)}$$

This fitting function, which is accurate to better than 0.5 per cent over the mass range $10^6 \leq M \leq 10^{16}\,h^{-1}\,\mathrm{M}_\odot$, is only valid for a spatial top-hat filter, and based on a power spectrum $P(k) = kT^2(k)$ [i.e. we assume that the initial power spectrum has a Harrison–Zeldovich form $P(k) \propto k$] with $T(k)$ the transfer function given by Bardeen et al. (1986):

$$T(k) = \frac{\ln(1 + 2.34q)}{2.34q} \times [1 + 3.89q + (16.1q)^2 + (5.46q)^3 + (6.71q)^4]^{-1/4}. \quad \text{(A11)}$$

Here $q = k/\Gamma$, with k in $h\,\mathrm{Mpc}^{-1}$.

APPENDIX B: AN ALTERNATIVE FORM FOR THE UNIVERSAL MASS ACCRETION HISTORY

After this paper was submitted, Wechsler et al. (2001, hereafter WBPKD) presented a similar investigation into the MAHs of CDM haloes. They used the exponential form

$$\Psi(M_0, z) = \mathrm{e}^{-\alpha z} \quad \text{(B1)}$$

to fit the mass accretion histories of individual haloes in a ΛCDM simulation. There are subtle differences between the fitting function suggested here and the one used by WBPKD, warranting a closer inspection of which, if any, provides a better fit. To that extent we have fitted the AMAHs of the 100 haloes (with different masses and different cosmologies) presented in Section 5 with the exponential MAH of equation (B1). In the left-hand panel of Fig. B1 we plot $\log(\chi^2_{\rm exp}/\chi^2_{\rm uni})$ as a function of $z_{\rm f}$. Here $\chi^2_{\rm exp}$ and $\chi^2_{\rm uni}$ correspond to the best-fitting values of χ^2 for the fitting functions of equations (B1) and (15), respectively. As can be seen, $\log(\chi^2_{\rm exp}/\chi^2_{\rm uni})$ and $z_{\rm f}$ are fairly strongly correlated to the extent that haloes that form relatively late ($z_{\rm f} \lesssim 1.5$) are on average better fitted by the universal MAH of equation (15), whereas the opposite is true for haloes that form early ($z_{\rm f} \gtrsim 1.5$).

In the right-hand panel of Fig. B1 we plot the best-fitting values of α as a function of the best-fitting values of $z_{\rm f}$. As can be seen there is a strong correlation between these two parameters, which is well fitted by

$$\alpha = \left(\frac{z_{\rm f}}{1.43}\right)^{-1.05} \quad \text{(B2)}$$

(solid line). The fact that α and $z_{\rm f}$ are so well correlated means that one can use equation (B2) and the recipe in Appendix A to estimate the value of α for the average MAH of a dark matter halo of arbitrary mass and cosmology. This can, for example, be used to improve accuracy by using equation (B1) instead of (15) as an analytical description for the AMAH of haloes with $z_{\rm f} \lesssim 1.5$.

Another advantage of having a direct way to compute α from the recipe outlined in Appendix A is that WBPKD have shown that α is strongly correlated with the concentration of the final halo; more concentrated haloes form on average earlier. WBPKD have shown that a good fit is obtained with $c_{\rm vir} = 8.2/\alpha$, where $c_{\rm vir} = r_{\rm vir}/r_{\rm s}$, with $r_{\rm vir}$ the virial radius of the halo and $r_{\rm s}$ the characteristic radius of the NFW (Navarro et al. 1997) halo density profile. Using the recipe in Appendix A and equation (B2), one can thus compute the *average* concentration of a dark matter halo of any mass and for any cosmology. There are two small caveats here. First of all, the relation between $c_{\rm vir}$ and α has only been tested for one cosmology (with $\Omega_0 = 0.3$, $\Omega_\Lambda = 0.7$, $h = 0.7$ and $\sigma_8 = 1.0$), and it remains to be seen whether this also holds for other cosmologies. However, since the results of WBPKD strongly suggest that the halo concentration is set entirely by its MAH (i.e. the scatter in $c_{\rm vir}$ for haloes of a fixed mass is consistent with the scatter in MAHs), it seems likely that this will be the case. Secondly, the relation between $z_{\rm f}$ and α of equation (B2) is based on EPS MAHs, whereas the relation between $c_{\rm vir}$ and α is based on MAHs fitted directly to simulations. Since the EPS MAHs and those extracted from simulations show some inconsistencies (see Section 4), there will

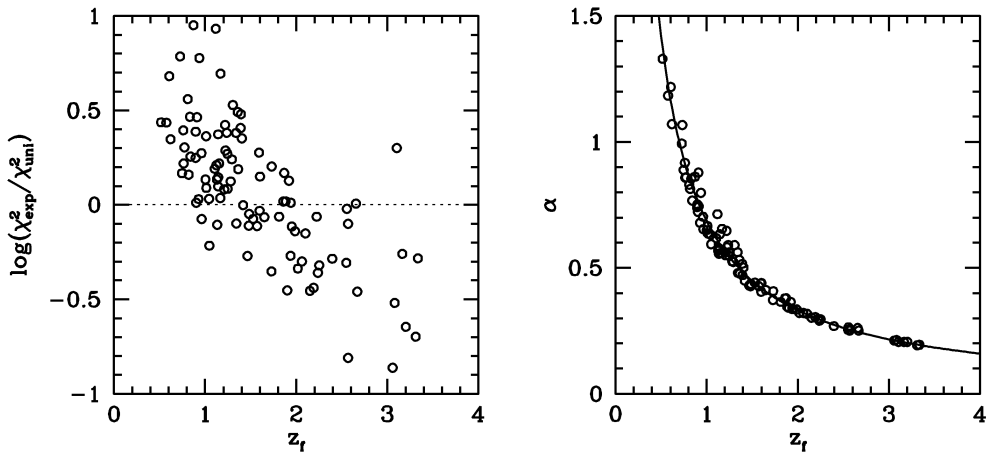

Figure B1. In the left-hand panel we plot the ratio of $\chi^2_{\rm exp}$ and $\chi^2_{\rm uni}$ as function of the best-fitting value of $z_{\rm f}$ for 100 haloes with different masses and in different cosmologies (see Section 5). As can be seen, on average $\chi^2_{\rm exp} > \chi^2_{\rm uni}$ for $z_{\rm f} < 1.5$, which implies that the universal fitting function of equation (15) provides a better fit to the AMAH of CDM haloes that form relatively late, whereas the exponential MAH of equation (B1) typically provides a better fit in cases with $z_{\rm f} > 1.5$. In the panel on the right we plot the best-fitting values of α versus the best-fitting values of $z_{\rm f}$, which are strongly correlated. The solid line corresponds to the fitting function of equation (B2), which can be used to convert $z_{\rm f}$ computed using the recipe in Appendix A to α.

be a systematic, but small, error in the values of $c_{\rm vir}$ thus derived. Since the discrepancy between EPS and simulations depends on mass and cosmology, the same applies for the amplitudes of these errors. Nevertheless, since for most cases the error will be relatively small compared with the scatter in $c_{\rm vir}$, this method allows one to compute halo concentrations for arbitrary halo mass and cosmology to sufficient accuracy for most purposes.

This paper has been typeset from a TEX/LATEX file prepared by the author.